MICROMECHANISMS AND LOCAL APPROACH OF FRACTURE IN A PEARLITIC STEEL

A. FONTAINE*, S. JEUNEHOMME*

The fracture mechanism of a coarse pearlitic steel has been investigated. The final cleavage fracture is due to the instability of fibrous cracks nucleated by shear cracking of the colonies. The increase of the stress triaxiality significantly reduces the critical length of the fibrous crack. A finite element mechanical analysis of the different specimens shows that the growth of the cavity in the pearlitic structure follows a law which is appreciably different from the one proposed by RICE and TRACEY. Finally, a local approach of the fracture of pearlitic steels is proposed, which takes into account the growth of the fibrous cracking.

INTRODUCTION

The fracture mechanisms of pearlitic steels have been widely studied. The main suggestion, by PARK and BERNSTEIN (1) is that ductile cracks nucleate by shear cracking, as proposed by MILLER and SMITH (2). It has been shown more recently that this mechanism only occurs in coarse pearlitic steels and is enhanced by the lower stress triaxiality situations or higher testing temperatures (KAVISHE and BAKER (3), (4), LEWANDOWSKI and THOMPSON (5), (6)). In the case of fine pearlitic microstructures, the cleavage fracture mechanism is the same as for ferritic steels, i.e. propagation-controlled. On the other hand, these various mechanisms observed on notched specimens cannot account for the effect of microstructure and temperature on fracture toughness measurements. It seems that the behaviour of the pearlitic steel at crack tip differs from the one observed in a lower stress triaxiality situation. Nevertheless, small notched specimens are more convenient for quality control and metallurgical studies than fracture mechanics ones.

* Centre Commun de Recherches, IRSID, 185 rue du Président Roosevelt, F-78100 SAINT-GERMAIN-EN-LAYE.

The objective of the present research is to exlain the change of fracture mechanism with stress triaxiality and to relate fractographic observations with a mechanical analysis in order to develop a local fracture criterion for pearlitic steels. This local approach of fracture derives from the models for cleavage and ductile fracture developed by PINEAU (7) and BEREMIN (8).

EXPERIMENTAL TECHNIQUES

This study has been carried out on a UIC 90A rail steel. The chemical composition and the conventional tensile properties are given respectively in tables 1 and 2. This steel presents a coarse pearlitic microstructure (mean austenitic grain diameter 100 µm, mean lamellar spacing 0.25 µm) and less than 1% of proeutectoïd ferrite veins. The tests specimens have been taken from the rail head, their tensile direction parallel to the rolling direction. Tensile smooth specimens (called TB5) and tensile circumferencially-notched specimens have been broken at room temperature. The geometries of the notched specimens are shown in figure 1. Four different notch radii have been chosen in order to change the stress triaxiality in the notched section. The micromechanisms of fracture are observed on cross-sectional surfaces, nital etched after electron-beam polishing.

TABLE 1 - Chemical composition of the steel studied (weight 10^{-5})

C	Mn	Si	S	P	Al	Ni	Cr	Cu	V
657	1 032	345	25	23	10	52	29	39	< 2

TABLE 2 - Conventional mechanical properties of the steel at room temperature

$\sigma_{0.2}$ (MPa)	σ_{UTS} (MPa)	R.A. (%)
470	931	19.0

FRACTOGRAPHIC AND MICROGRAPHIC OBSERVATIONS

The fracture surfaces examined showed that fracture occurred macroscopically by different mechanisms. The most sharply notched specimens AE 0.1 exhibit fully transgranular cleavage whereas an increasing amount of ductile tearing is observed as the stress triaxiality decreases. In the case of the smooth tensile specimens TB5, the fibrous crack extends on half the diameter at rupture

(figure 2). In the ductile area the role of the pearlitic structure appears clearly on the fracture surface (figure 3a), while larger cavities, nucleated from Mn S inclusions grow up to the coalescence with those nucleated from the cementite (figure 3b).

The different stages of this fibrous cracking were observed on polished sections of specimens on which interrupted tests have been performed. The first cracks appear just before the final cleavage fracture. A large fibrous crack (> 100 µm) can thus be observed in the centre of the specimen by interrupting tests at more than 95% of fracture displacement, after necking (figure 4). In this case, a lot of shorter cracks (≤ 20 µm) are observed in the necked section, more than 75% of them in the colonies located in a plane parallel to the tensile direction and with their length at a 45° angle from this direction.

This preferential cracking of the colonies parallel to the tensile direction, observed by KURITA et al. (9), is the rule (figure 5a). This photograph also shows that the MnS inclusions do not play a significant part due to their orientation. The slip bands generated in the ferrite are arrested by the colony boundaries (figure 5b). These individual colony cracks coalesce to form the critical defect for cleavage fracture. Colony boundaries perpendicular to the tensile direction do not act as crack barrier but can be the weakest point of the structure (figure 6a). The proeutectoïd ferrite veins always act as crack starter (figure 6b); due to their lower tensile properties, these veins are submitted to high local stress triaxiality.

MECHANICAL ANALYSIS

Table 3 gives the average values of the measured mechanical parameters for the five groups of specimens. The overall strain at fracture is defined as $\bar{\varepsilon}_F = 2 \ln \emptyset_0/\emptyset_F$ and the overall fracture stress as $\bar{\sigma}_F = 4 P_F/\pi\emptyset_F^2$. It can be seen that the ductility decreases when the notch radius is increased whereas the overall cleavage stress increases. In the case of the AE 0.1 specimens, this stress is no longer representative because of the steep stress gradient, similar to a crack tip situation.

Finite-element calculations of these specimens have been carried out [10]. The main results of this numerical approach is that the stress triaxility σ_m/σ_{eq} is maximum in the centre of the specimens except for the AE 0.1 where its maximum is 200 µm ahead of the notch tip.

TABLE 3 - Average mechanical parameters at fracture

Type of specimen	TB5	AE 6.4	AE 2.5	AE 1.25	AE 0.1
$\bar{\varepsilon}_F$ (%)	21.1	12.2	11.2	9.2	0.16
$\bar{\sigma}_F$ (MPa)	1 108	1 278	1 338	1 436	832

It has been shown that the cleavage fracture of this pearlitic steel is initiated by ductile tearing, at least for the lower stress-triaxiality situations. RICE and TRACEY (11) have derived a relationship for the growth of a spherical cavity in an infinite plastic material. In order to allow for work-hardening, the equivalent VON MISES stress is taken as the yield stress (7):

$$\ln (R/R_o) = 0.283\ \varepsilon_{eq} \exp (1.5\ \sigma_m/\sigma_{eq}) \quad \ldots\ldots\ldots\ldots [1].$$

This relationship does not apply directly to a pearlitic steel because the main hypotheses (spherical voids, no interaction between inclusions) are not fulfilled. Following (7), if the fracture mechanism remains the same, the cavity growth at fracture, derived from the equation above, reaches a constant value $\ln (R/R_o)_c$. The stress and strain fields at fracture in the notched specimens have been evaluated by a finite-element method (11), and by BRIDGMANN formulae (12) for the smooth specimens TB5.

The stress triaxiality is the main controlling parameter for cavity growth. The local equivalent VON MISES strain at fracture at the location where the triaxiality is maximum has been reported in figure 7 as a function of the maximum value of the triaxiality. As expected, this figure shows a relationship appreciably different from [1]:

$$\ln (R/R_o) = \alpha\ \varepsilon_{eq} \exp (2.85\ \sigma_m/\sigma_{eq}) \quad \ldots\ldots\ldots\ldots\ldots [2].$$

In particular, the influence of the stress triaxiality is twice as important as the one that predicted by RICE and TRACEY.

DISCUSSION: PROPOSAL OF A LOCAL CRITERION OF FRACTURE

The cleavage fracture of this pearlitic steel is initiation-controlled. The fibrous crack becomes unstable when its length is such that:

$$\sigma_c \approx \left[\frac{E\ \delta_s}{2R}\right]^{1/2} \quad \ldots\ldots\ldots\ldots\ldots\ldots\ldots\ldots [3].$$

R is not an unknown random variable, it increases from the cavities induced by shear cracking of the cementite lamellae following [2], where R_o can be taken as the lamellae thickness.

The local criterion is not a critical stress but can be expressed as $\sigma \sqrt{R}$. The scatter encountered during testing tensile or pre-cracked specimens is due to the random distribution of the colonies in the fracture process zone. Indeed, it has been shown previously that fibrous cracking occurred preferentially in the colonies parallel to the principal tensile direction. Finally, the failure probability of the hole specimen will be expressed as in the BEREMIN model (8):

$$P_R = 1 - \exp\left[- \int_{Vd} p(\sigma, R) \frac{dV}{V_o} \right] \quad \ldots\ldots\ldots\ldots\ldots\ldots\ldots\ldots [4]$$

where $p(\sigma, R)$ is the failure probability of the elementary volume and V_d the volume where ductile tearing occurs.

For low triaxial situations, the unstable fibrous crack length is very large with respect to the element size. In this case, this local criterion will not be accurate because the elementary volumes are not independent (8). On the contrary, this criterion will apply more precisely for fine pearlitic microstructures, for which fracture is more propagation-controlled (3).

SYMBOLS USED

E = YOUNG modulus

P_F = fracture load of the tensile specimen

R = radius of the fibrous crack (R_o initial value)

V_o = elementary volume of BEREMIN model (8)

δ_s = effective surface energy of the steel

$\emptyset$ = diameter of the tensile specimen ($\emptyset_o$ initial, $\emptyset_F$ at fracture)

ε_{eq} = equivalent VON MISES plastic strain

σ_m = hydrostatic stress

σ_{eq} = equivalent VON MISES stress

REFERENCES

(1) Park Y.J. and Bernstein I.M. in ASTM STP 644, 1978, pp. 287-332.

(2) Miller L.E. and Smith G.S., J.I.S.I., vol. 208, 1970, pp. 998-1005.

(3) Kavishe F.P.L. and Baker T.J., in "Fracture Control of Engineering Structures" (E.C.F. 6), edited by Van Elst H.C. and Bakker A., EMAS, 1986, vol. 3, pp. 1721-1737.

(4) Kavishe F.P.L. and Baker T.J., Mat. Sci. and Tech., vol. 2, 1986, pp. 583-588.

(5) Lewandowski J.J. and Thompson A.W., Met. Trans. A, vol. 17 A, 1986, pp. 461-472.

(6) Lewandowski J.J. and Thompson A.W., Met. Trans. A, vol. 17 A, 1986, pp. 1769-1786.

(7) Pineau A., in "Advances in Fracture Research" (I.C.F.5.), edited by François D. Pergamon, 1981, vol. 2, pp. 553-577.

(8) Beremin F.M., Met. Trans. A, vol. 14 A, 1983, pp. 2277-2287.

(9) Kurita Y., Roesch L. and Sanzay C., Mém. Scient. Revue Métallurgie, 1977, pp. 731-756.

(10) Fontaine A., Jeunehomme S., to be published.

(11) Rice J.R. and Tracey D.N., J. Mech. Phys. Solids, vol. 17, 1969, pp. 201-217.

(12) Bridgmann, "Large Plastic Flow and Fracture", Mc Graw Hill, 1952.

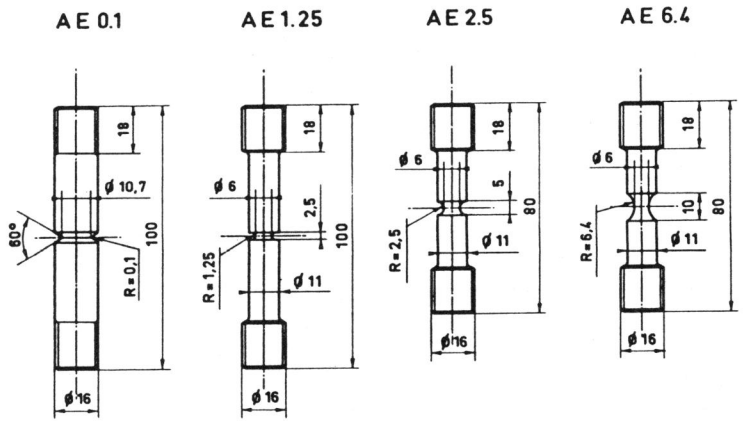

Figure 1 Geometries and dimensions of the notched tensile specimens

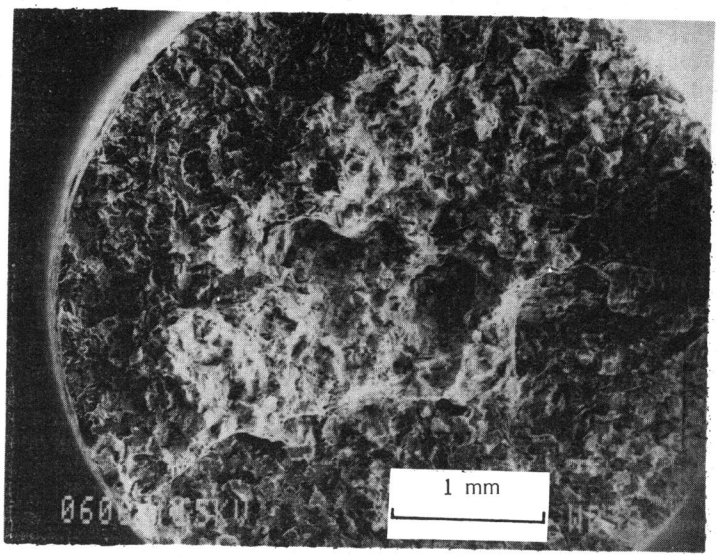

Figure 2 Spreading of the fibrous crack in the centre of a smooth tensile specimen

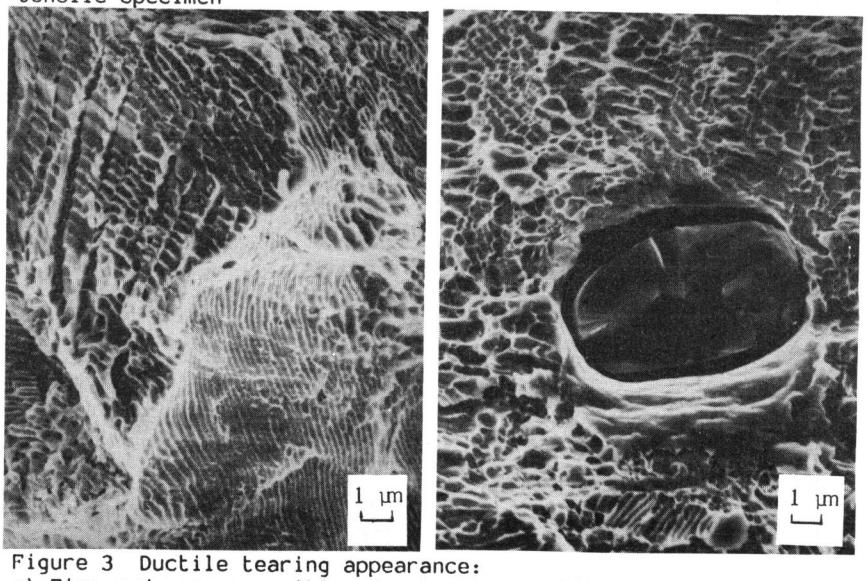

Figure 3 Ductile tearing appearance:
a) Fine and coarse cavities due to the pearlitic structure,
b) Growth of a large cavity from an MnS inclusion

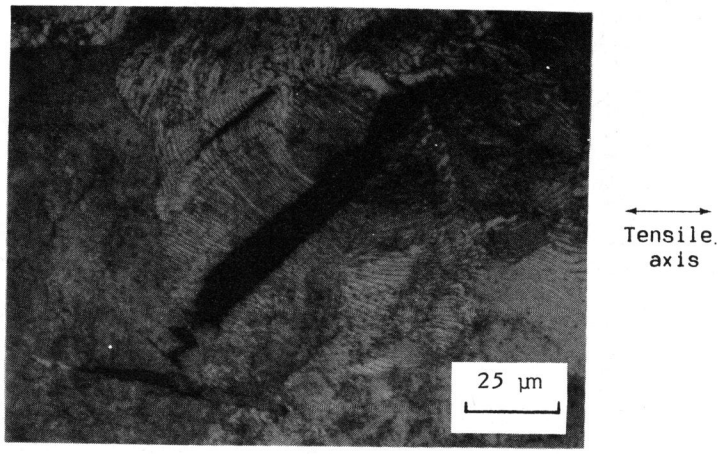

Figure 4 Large fibrous crack observed in a smooth tensile specimen just before cleavage instability. Note the coalescence with the inclusion cavity.

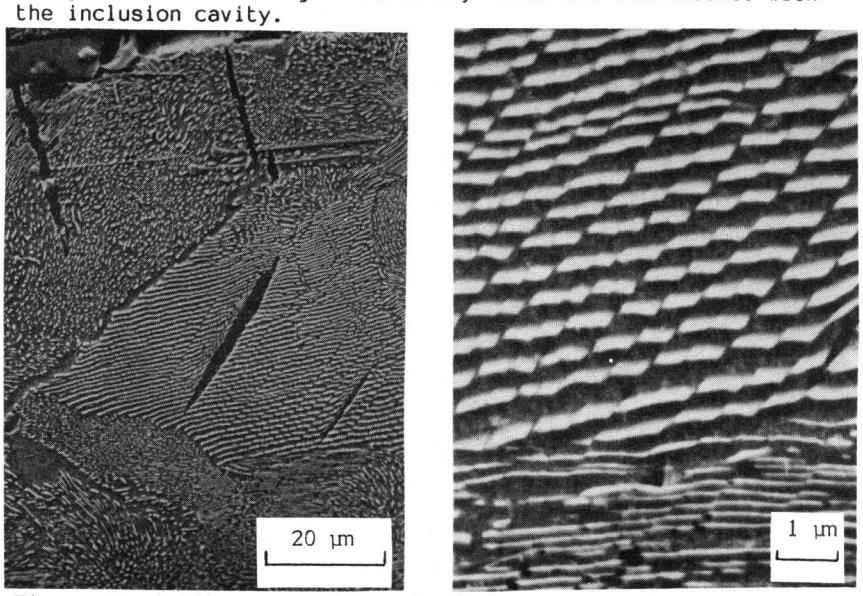

Figure 5 a) Fibrous cracking of the colonies parallel to the tensile direction (←→), b) Arrest of the slip bands at the colony boundaries

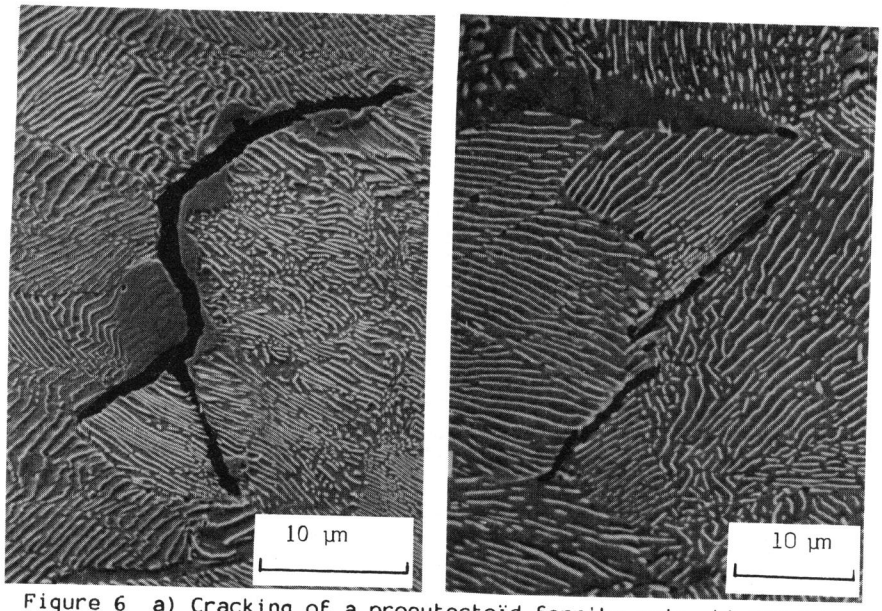

Figure 6 a) Cracking of a proeutectoïd ferrite vein, b) Cracking of a colony boundary due to its orientation with respect to tensile axis (⟷)

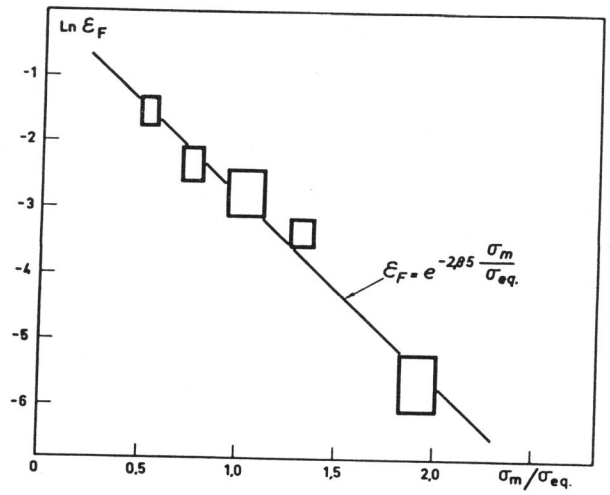

Figure 7 Relationship between the maximum value of the stress triaxiality and the equivalent VON MISES strain at the location where the triaxiality is maximum